Research Square

Preprints are preliminary reports that have not undergone peer review.
They should not be considered conclusive, used to inform clinical practice,
or referenced by the media as validated information.

Metal cofactor level chassis engineering enables aerobic expression of tungsten formate dehydrogenases in Escherichia coli

Yong Hwan Kim

metalkim@unist.ac.kr

UNIST https://orcid.org/0000-0003-4729-693X

Uyen Phan

Jun-Min Lee

Korea University

Toan Vo

UNIST

Min-Kyu Oh

Korea University https://orcid.org/0000-0001-6406-3930

Article

Keywords: Formate dehydrogenase, Tungsten cofactor, W-bis-MGD, Tungstate transport, Iron–sulfur cluster, CO_2 reduction, Synthetic chassis

Posted Date: February 23rd, 2026

DOI: https://doi.org/10.21203/rs.3.rs-8913862/v1

License: This work is licensed under a Creative Commons Attribution 4.0 International License.
Read Full License

Additional Declarations: There is **NO** Competing Interest.

Abstract

Tungsten-dependent formate dehydrogenases catalyze CO_2 reduction, yet their heterologous production remains limited by the absence of tungsten-specific cofactor maturation in standard laboratory hosts. Although molybdenum-dependent formate dehydrogenases have been implemented in *Escherichia coli*, analogous maturation of tungsten-dependent enzymes has proven unsuccessful because native metal homeostasis does not support selective tungstate uptake or W-bis-MGD assembly. Here we reconstitute tungsten-specific metal metabolism in *E. coli* by reconstructing tungsten cofactor biosynthesis, installing a high-affinity tungstate uptake system, and reinforcing Fe–S cluster biogenesis. This enables aerobic production of catalytically competent tungsten-dependent formate dehydrogenase from *Methylorubrum extorquens* AM1, achieving native-level specific activity and a tungsten occupancy of 0.92 mol per mol enzyme—nearly double that of the native host. The engineered strain delivers a volumetric activity exceeding 3,500 U L^{-1}. In a coupled whole-cell CO-to-formate biotransformation, the strain generated 44 mM formate within 4 hours, outperforming the native host system by more than threefold. The platform also supports activation of W-bis-MGD-dependent enzymes from *Cupriavidus necator* H16 and *Lutibaculum baratangense* AMV1. This work establishes a general design framework for W-bis-MGD maturation, expanding access to tungsten-dependent biocatalysts for CO_2-to-formate and related reductive biotransformations.

Introduction

Carbon dioxide (CO_2) conversion has become a cornerstone of climate-aligned manufacturing, enabling fixation and valorization of a major greenhouse gas into valuable chemicals[1]. Among CO_2-derived products, formate is particularly attractive because it can be produced from CO_2 with high energy efficiency using technically straightforward routes[2] and already supports a mature market with established applications across chemical and agricultural sectors[3]. Motivated by rising atmospheric CO_2 levels and increasingly stringent decarbonization targets, these advantages have intensified efforts to develop selective, low-energy CO_2-to-formate platforms that integrate biological systems with renewable power, thereby accelerating the transition from carbon capture to circular utilization[4, 5, 6].

Among available biocatalysts, formate dehydrogenases (FDHs) incorporating high-valent transition metal cofactors, most prominently molybdenum (Mo) and tungsten (W), have emerged as leading candidates for CO_2-to-formate conversion due to their high catalytic efficiency, favorable thermodynamics, and broad applicability in C1-based biomanufacturing[4, 7, 8]. Although Mo- and W-dependent FDHs share a conserved bis-molybdopterin guanine dinucleotide (bis-MGD) framework, the identity of the central metal atom profoundly affects catalytic behaviors. The tungsten center in W-FDHs exhibits a substantially lower redox potential than its molybdenum counterpart, expanding the low-potential operational window and enhancing hydride-transfer kinetics. As a result, W-FDHs thermodynamically favor the reductive conversion of CO_2 to formate, making them particularly suitable for CO_2 fixation and bio-electrochemical CO_2 reduction[7, 9, 10, 11, 12, 13].

Despite these advantages, the broader deployment of W-FDHs has been constrained by fundamental challenges in heterologous maturation. Although *Escherichia coli* can support recombinant expression of Mo-FDHs by leveraging its native molybdenum cofactor (Moco) biosynthesis pathway[14, 15], analogous functional expression of authentic tungsten-dependent enzymes in this host has proven much more difficult. While recent studies have demonstrated *E. coli*–based implementations of metalloenzyme modules for CO_2 reduction and formate-driven C1 metabolism[16, 17], a broadly applicable aerobic, chassis-level solution that enables efficient tungsten-selective maturation of W-bis-MGD enzymes in *E. coli* has remained limited.

These limitations arise from intrinsic features of *E. coli* metal homeostasis. Moreover, tungsten-dependent enzymes impose additional constraints[18], including competition between molybdenum and tungsten for cofactor metalation, stringent control of tungstate availability, and reliance on iron–sulfur (Fe–S) cluster biogenesis. These processes are not inherently aligned with native *E. coli* physiology. As a result, heterologous expression of tungsten-containing oxidoreductases in *E. coli* frequently yields incomplete cofactor incorporation, metal misallocation, or catalytically inactive apoenzymes[19, 20, 21].

Here, we engineered a W-bis-MGD-cofactor–competent *E. coli* chassis through coordinated reprogramming of intracellular tungsten metabolism and Fe-S cluster assembly. This strategy combined reconstruction of tungsten-cofactor biosynthesis using key genes from *Methylorubrum extorquens* AM1, chromosomal integration of a high-affinity tungstate transporter (TupBCA*)* from *Sulfitobacter dubius* NA4, and genomic reinforcement of Fe–S cluster biogenesis via targeted engineering of the *isc* operon. The resulting chassis supports soluble, catalytically active expression of multiple W-dependent enzymes under aerobic conditions, including MeFDH1 from *M. extorquens* AM1, CnFDW from *Cupriavidus necator* H16, and a structurally predicted LbFDH from *Lutibaculum baratangense* AMV1.

By overcoming tungsten-specific maturation barriers in a host previously considered incompatible with W-enzyme assembly, this work converts E. coli into a programmable platform for W-bis-MGD enzyme production. The approach establishes a transferable design framework for aerobic maturation of tungsten-dependent redox enzymes and expands access to this underexplored metallocofactor chemistry for sustainable CO_2 reduction and related reductive biotransformations.

Results

Reconstitution of W-bis-MGD biosynthesis restores MeFDH1 activation in E. coli

The tungsten-dependent formate dehydrogenase from *Methylorubrum extorquens* AM1 (MeFDH1) was selected as a stringent tungsten-dependent model oxidoreductase, as its catalytic activity strictly requires W-bis-MGD metalation. However, recombinant expression of MeFDH1 in *Escherichia coli* does not yield catalytically competent enzyme[22], indicating that this host lacks a tungsten-compatible maturation environment. We therefore sought to reconstruct the cognate tungsten-specific cofactor

biosynthetic machinery from *M. extorquens* AM1 in *E. coli* to establish a tungsten-dependent maturation pathway (Fig. 1).

Prior genetic characterization of MeFDH1 maturation in *M. extorquens* AM1 (summarized in Supplementary **Table S1**) identified MoeA1, MobA, MobB, and FdhD as essential components of the native W-bis-MGD biosynthetic pathway. Among the five annotated *moeA* homologs, only *moeA1* in *M. extorquens* AM1 was required for MeFDH1 activity, establishing MoeA1 as the sole tungsten-specific insertion factor for this enzyme. Deletion analyses further showed that *mobB* and *fdhD* are required for MeFDH1 activity, whereas *mobA* is essential for bis-MGD biosynthesis in the native host. These findings defined the minimal tungsten-specific maturation module guiding heterologous reconstruction.

To assess potential coordination among these factors in the context of reconstruction, protein–protein interactions were evaluated using a bacterial adenylate cyclase two-hybrid (BACTH) assay (Supplementary **Fig. S1**). MoeA1 exhibited reproducible interactions with both MobA and MobB, while FdhD interacted preferentially with the Mob protein rather than directly with MoeA1. Collectively, this interaction pattern is consistent with a cooperative engagement of these factors during W-bis-MGD maturation and provides contextual support for the reconstruction strategy, as schematically summarized in Fig. 2a.

Guided by these observations, *moeA1*, *mobA*, *mobB*, and *fdhD* from *M. extorquens* AM1 were codon-optimized and cloned into a pCDFDuet-1 vector under separate T7 promoters (Table 1). In parallel, the MeFDH1 α and β subunits were codon-optimized and cloned into a pETDuet-1 expression vector. *E. coli* BL21(DE3) was then co-transformed with MeFDH1 and various combinations of the tungsten cofactor (Wco) biosynthetic genes to assess their individual and combinatorial contributions to enzyme activation.

As expected, expression of MeFDH1 alone (BL) resulted in negligible activity (< 1 U mg^{-1}), indicating predominant accumulation of apoenzyme due to insufficient availability of the W-bis-MGD cofactor. Similarly, strains expressing individual Wco genes, *moeA1* (W1), *mobA* (WA), or *mobB* (WB), failed to produce measurable activity (Fig. 2b), demonstrating that no single component is sufficient to support cofactor assembly or enzyme activation. Although MoeA1 is strictly required for MeFDH1 function in the native host, its expression alone was insufficient to restore activity in the heterologous background.

The recovery of measurable activity (~ 6 U mg^{-1}) in the *moeA1–mobB* strain (W2) indicates that cooperative expression of these two proteins is sufficient to enable functional tungsten cofactor maturation in *E. coli*. Introduction of *mobA* into the *moeA1–mobB* background (W3) led to a substantial increase in activity, suggesting that bis-MGD formation markedly enhances catalytic competence once tungsten has been integrated into the cofactor. Conversely, removal of *mobB* from the W3 background abolished MeFDH1 activity (Supplementary **Fig. S2**) indicating that MobB is required for productive W-bis-MGD maturation. Finally, inclusion of *fdhD* (W4) yielded the highest activity (~ 27 U mg^{-1}) and was accompanied by an approximately threefold increase in tungsten occupancy relative to the MeFDH1-only background (Table 2), consistent with improved completion of cofactor maturation. Accordingly, the full

four-gene module (*moeA1*, *mobA*, *mobB*, and *fdhD*) was adopted as the standard Wco biosynthetic configuration for all subsequent experiments.

The progressive enhancement in activity from W2 to W4 is consistent with the interaction relationships detected by BACTH analysis and supports a coordinated maturation process in which functional W-bis-MGD biosynthesis in *E. coli* requires the integrated action of multiple pathway components rather than expression of individual biosynthetic genes. Nevertheless, the maximal activity achieved in *E. coli* remained substantially lower than that observed in *M. extorquens* AM1 (~ 50 U mg^{-1}), suggesting the presence of additional constraints, including limitations in tungsten uptake and iron–sulfur (Fe–S) cluster availability. This establishes the minimal tungsten maturation module.

Selective tungstate transport enhances tungsten incorporation and enzyme performance

Consistent with the residual activity gap observed after W-bis-MGD pathway reconstruction, MeFDH1 produced with the W4 module exhibited limited tungsten occupancy (~ 27% of theoretical stoichiometry). This incomplete loading suggested that tungsten availability, rather than cofactor assembly capacity alone, may constrain effective W-bis-MGD biosynthesis in *E. coli*. Given that BL21(DE3) lacks the high-affinity ModABC molybdate/tungstate transport system present in K-12 derivatives[23, 24], we next examined whether enhanced tungstate uptake could alleviate this limitation.

Three candidate transport systems were evaluated by plasmid expression in tungstate-supplemented cultures, including the *E. coli* K-12 *modABC* operon, the tungsten-specific *tupBCA* operon from *Sulfitobacter dubius* NA4[25, 26], and the *tupBCA* operon from *M. extorquens* AM1[27]. Among these, the *S. dubius* NA4–derived TupBCA produced the highest MeFDH1 specific activity, outperforming both ModABC from *E. coli* K-12 and the *M. extorquens* TupBCA (Supplementary **Fig. S3**). Based on this performance and to minimize plasmid burden in downstream experiments, the *S. dubius* NA4 transporter was integrated into the chromosome of *E. coli* BL21(DE3) under control of a T7 promoter, generating strain BL1 (Table 1).

The selected *tupBCA* operon from *S. dubius* NA4 encodes an ATP-binding cassette (ABC)–type tungstate transporter composed of the periplasmic binding protein TupA, membrane permease TupB, and ATPase TupC[26]. Co-expression of the genomically integrated transporter with the W4 biosynthetic module resulted in a substantial increase in MeFDH1 activity (~ 35 U mg^{-1}) and improved soluble protein yield (~ 2.0 mg g^{-1} WCW) (Fig. 3). Tungsten incorporation increased by approximately twofold in MeFDH1 purified from transporter-containing strains, reaching ~ 50% of the theoretical stoichiometry (Table 2), representing a substantial improvement over the transporter-deficient controls.

To further assess the metal selectivity of the reconstructed tungsten cofactor biosynthetic pathway, MeFDH1 activity and metal profiling were examined under three conditions: tungstate alone (1 mM), mixed tungstate (0.5 mM) and molybdate (0.5 mM), or molybdate alone (1 mM). Cultures supplied

exclusively with tungstate produced the highest MeFDH1 activity (~ 35 U mg^{-1}), whereas mixed-metal conditions led to a marked reduction in activity (~ 10 U mg^{-1}). No activity was observed under molybdate-only supplementation.

Metal quantification showed that tungsten incorporation was highest under tungstate-only conditions (~ 0.51 mol W per mol enzyme) and decreased under mixed-metal supplementation, while molybdenum incorporation remained negligible across all treatments (Supplementary **Table S2**). The minimal Mo occupancy suggests that molybdenum does not efficiently substitute for tungsten in the mature enzyme population. Instead, the reduced activity under mixed conditions likely reflects competitive interference during metal allocation or early stages of W-bis-MGD biosynthesis, which impairs efficient cofactor assembly without substantial Mo incorporation into the purified enzyme.

These results reveal that W-bis-MGD assembly in BL21(DE3) is highly sensitive to intracellular metal balance, as even modest molybdate supplementation can disrupt selective tungsten incorporation. Enhancing high-efficiency tungsten transport therefore promotes effective cofactor assembly and improved enzyme performance. These findings identify tungsten transport as a primary bottleneck in this host and establish dedicated tungstate acquisition as a critical design element for reliable expression of tungsten-dependent enzymes in synthetic systems.

Reinforcement of iron-sulfur cluster biogenesis increases metalation and yield

Beyond the W-bis-MGD cofactor at the active site, MeFDH1 relies on multiple iron–sulfur (Fe–S) clusters in both the α and β subunits to mediate electron transfer to physiological and artificial electron acceptors such as NADH or ethyl viologen (EV) (Supplementary **Fig. S4**). In *E. coli*, Fe–S cluster biosynthesis is mediated primarily by the ISC and SUF systems, with ISC tightly regulated by the global repressor IscR[28, 29]. While sufficient for native metabolism, IscR-mediated regulation may not meet the elevated Fe–S cluster demand imposed by overexpression of multi–Fe–S enzymes such as MeFDH1. Consistent with this limitation, MeFDH1 produced prior to *isc* engineering contained only ~ 20–25% of the theoretical iron content (~ 20 mol Fe per mol enzyme; Table 2), indicating extensive under-metalation.

In addition to delivering Fe–S cluster to target proteins, the ISC machinery has been implicated in bis-MGD cofactor biosynthesis in bacteria. Specifically, IscA functions as an Fe–S carrier that transfers clusters to MoaA, which catalyzes the first step of MPT synthesis, while IscS serves as a sulfur donor that regulates the synthesis rate[30, 31]. Enhanced ISC activity is therefore expected to support not only Fe–S cluster assembly but also W-bis-MGD biosynthesis[32].

To test this hypothesis, we first enhanced Fe–S biosynthesis by plasmid-based co-expression of the *isc* operon using pRKISC[33]. Introduction of pRKISC into BL1 moderately improved MeFDH1 specific activity (46 U mg^{-1}) and soluble yield (4.5 mg g^{-1} WCW), approaching levels observed the native *M. extorquens*

AM1 (Fig. 4). We next implemented genome-level upregulation of endogenous Fe–S biogenesis by deleting *iscR* and replacing the native *isc* promoter with a strong synthetic promoter (P_{trc}), generating strain BL2 (Table 1). In BL2, MeFDH1 exhibited near-native specific activity (~ 48 U mg^{-1}) and substantially increased soluble yield (~ 10 mg g^{-1} biomass), corresponding to a total volumetric activity exceeding 3500 U L^{-1}, approximately 15-fold higher than native AM1 (~ 240 U L^{-1}) and surpassing reported productivity in *Cupriavidus necator* H16[19].

A potential concern associated with global reprogramming of metal homeostasis is unintended metabolic burden or impaired cellular fitness. Growth profiling (Supplementary **Fig. S5**) showed that plasmid-based overexpression of the *isc* operon moderately reduced maximal cell density, consistent with increased metabolic load. In contrast, genome-level reinforcement of Fe–S biosynthesis in BL2 restored and further improved growth relative to the plasmid-based strain, indicating that chromosomal integration enables more balanced expression of maturation machinery. Importantly, no severe growth defects were observed under production conditions, suggesting that coordinated reconstruction of tungsten transport, cofactor assembly, and Fe–S biogenesis is physiologically tolerated. The improved growth of BL2 likely contributes to its enhanced volumetric productivity by supporting greater biomass accumulation alongside increased intracellular abundance of fully active enzymes.

Elemental analysis confirmed functional improvements by revealing substantially enhanced metal content in MeFDH1 purified from the BL2 strain (Table 2). Iron occupancy increased from ~ 5 mol Fe mol^{-1} enzyme in BL1 to ~ 11 mol in BL2, closely matching the level observed for enzyme purified from native AM1. Although structural annotation predicts ~ 20 mol Fe mol^{-1} enzyme, both native and engineered preparations exhibited lower measured values, suggesting incomplete biogenesis or oxidative loss during aerobic purification step. Notably, MeFDH1 purified from *E. coli* BL2 displayed 92% tungsten occupancy, substantially higher than the 50% observed in native *M. extorquens* AM1 host. These coordinated increases in iron and tungsten incorporation are consistent with improved Fe–S cluster biogenesis in the engineered strain and support a functional link between Fe–S assembly and efficient W-bis-MGD maturation.

Together, these findings indicate that bis-MGD cofactor synthesis remains tightly coupled to cellular Fe–S assembly capacity, even when molybdenum is replaced by tungsten. Successful production of fully metalated tungsten enzymes therefore requires not only reconstruction of tungsten-selective transport and cofactor biosynthesis, but also sufficient Fe–S cluster assembly to sustain both catalytic function and cofactor maturation. These results identify Fe–S supply as a critical remaining constraint and directly link Fe–S capacity to efficient W-bis-MGD maturation.

Preservation of MeFDH1 catalytic competence in the engineered E. coli chassis

To determine whether the engineered chassis preserves intrinsic catalytic properties, kinetic parameters for CO_2 reduction were measured using purified MeFDH1 from engineered *E. coli* BL2 and the native *M. extorquens* AM1 host (Table 3). Under CO_2-dependent conditions, turnover numbers (kcat) were

comparable between BL2- and AM1-derived enzymes (141 s^{-1} vs 152 s^{-1}), indicating preserved catalytic turnover following heterologous maturation. Although the apparent K_M for CO_2 was moderately increased in BL2 (8.4 mM vs 3.6 mM), overall catalytic competence remained within the same order of magnitude, consistent with a modest decrease in substrate affinity rather than impaired catalytic chemistry. Similar trends were observed for EV-dependent measurements, where kcat values were largely maintained between preparations (304 s^{-1} vs 325 s^{-1}), with modestly elevated K_M values resulted in reduced catalytic efficiency in BL2. These data indicate that tungsten-specific cofactor reconstruction and enhanced Fe–S maturation in *E. coli* support formation of a catalytically competent enzyme without compromising turnover chemistry of MeFDH1.

Whole-cell CO-to-formate conversion demonstrates system-level impact

We next examined whether enhanced tungsten maturation translates into improved carbon conversion at the whole-cell level. A coupled CO-to-formate system was constructed in which *E. coli* expressing ChCODH (carbon monoxide dehydrogenase from *Carboxydothermus hydrogenoformans*) to oxidizes CO to CO_2 and generate reduced ethyl viologen ($EV^{\bullet+}$), which subsequently transfers electrons to MeFDH1-expressing cells to drive CO_2 reduction (Fig. 5a). Under matched biomass conditions, MeFDH1 produced in engineered BL2 generated 44 mM formate within 4 h, compared to 13 mM using enzyme derived from the native AM1 host (Fig. 5b), corresponding a ~ 3.5-fold increase in final titer and a markedly higher apparent production rate. Given the comparable intrinsic kinetic parameters of purified enzymes, the improved whole-cell productivity observed with BL2-derived MeFDH1 therefore is attributable to the higher intracellular abundance of tungsten-metalated MeFDH1 in the engineered chassis.

Engineered chassis supports heterologous expression of diverse tungsten-containing enzymes

Having established efficient tungsten-selective maturation and enhanced catalytic performance with MeFDH1, we next assessed whether the engineered chassis supports functional assembly beyond its original native context. To this end, we expressed CnFDW from *C. necator* H16, a characterized W-FDH previously produced in *M. extorquens* PA1[34]. In parallel, we identified a putative FDH from *Lutibaculum baratangense* AMV1 (LbFDH) through Foldseek-based structure homology analysis[35], which exhibits high structural similarity to characterized W-FDHs despite limited sequence identity (Supplementary **Fig. S6**).

As summarized in Table 4, the engineered BL2 chassis enabled functional expression of heterologous W-bis-MGD enzymes beyond MeFDH1. Expression of CnFDW in wild-type *E. coli* BL21(DE3) yielded no detectable activity, consistent with the absence of tungsten cofactor biosynthetic capacity. In contrast, CnFDW produced in BL2 exhibited substantial tungsten incorporation (~ 0.9 mol W per mol enzyme), confirming effective W-bis-MGD biosynthesis and insertion in the engineered host. Although full

theoretical occupancy was not achieved, the high tungsten loading was sufficient to support maximal catalytic activity (~ 30 U mg^{-1}), comparable to values reported for expression in *M. extorquens* PA1[34].

A similar pattern was observed for the structure-predicted LbFDH, which was inactive in BL21(DE3) but exhibited measurable activity accompanied by stoichiometric tungsten incorporation when expressed in BL2 (Table 4). The measured tungsten content (1.17 mol W per mol enzyme) slightly exceeded the theoretical maximum (1.0), likely reflecting minor uncertainties in protein quantification or normalization for this previously uncharacterized enzyme. Nevertheless, the high tungsten occupancy confirms successful W-bis-MGD assembly and insertion into a structurally predicted enzyme, demonstrating that the reconstructed metal-cofactor network supports proper metalation beyond well-studied FDHs. The comparatively lower activity of LbFDH likely reflects intrinsic structural features, differences in native electron-transfer partners, or suboptimal folding in the heterologous host, rather than incomplete cofactor assembly.

These results indicate that the engineered *E. coli* BL2 chassis is capable of efficiently maturing multiple W-FDHs under aerobic conditions, including both previously characterized proteins and structure-guided candidates. The transferable activation and high tungsten occupancy observed across distinct enzyme backgrounds suggest that the principal barrier to heterologous expression lies in host metal homeostasis rather than intrinsic enzyme incompatibility.

Discussion

The successful heterologous expression of MeFDH1 in *Escherichia coli* reported in this study addresses persistent challenges in the production of tungsten-containing metalloenzymes and demonstrates that tungsten-dependent enzyme maturation is not intrinsically incompatible with this host. Instead, functional expression is limited by the absence of an appropriately configured metal–cofactor environment. Our findings show that protein overexpression alone is insufficient when cofactor biosynthesis, metal selectivity, and auxiliary maturation pathways are not aligned with catalytic requirements. By integrating W-bis-MGD biosynthesis, tungsten-specific transport, and reinforcing Fe–S cluster assembly within a coordinated framework, we enabled aerobic maturation of non-native tungsten-dependent enzymes in *E. coli* through genome-level rewiring of trace-metal allocation.

Systematic reconstruction of the W-bis-MGD biosynthetic machinery revealed that functional activation required cooperative action of MoeA1, MobA, MobB, and FdhD, consistent with an integrated maturation network rather than a linear insertion sequence. The progressive restoration of activity and corresponding increases in tungsten occupancy identify cofactor availability and maturation efficiency as principal bottlenecks in heterologous expression of tungsten-dependent oxidoreductases. In this context, MoeA1 and MobB promote early cofactor formation, MobA enhances bis-MGD synthesis to elevate catalytic competence, and FdhD contributes to completion of the mature tungsten cofactor; these roles echo the cooperative biosynthetic roles described for molybdenum cofactor assembly in

bacteria[36, 37]. These observations underscore W-bis-MGD cofactor biogenesis as a coordinated system rather than a set of isolated enzymatic steps.

Metal discrimination emerged as a central yet often underappreciated challenge in heterologous metalloenzyme engineering. Tungsten and molybdenum, as closely related group 6 oxyanions, compete for overlapping transport and cofactor assembly pathways[38, 39], imposing stringent demands on selective uptake and insertion systems. To address this constraint, chromosomal integration of the high-affinity tungstate transporter from *Sulfitobacter dubius* NA4 (TupBCA) substantially increased tungsten incorporation and catalytic activity. Notably, MeFDH1 purified from the engineered *E. coli* BL2 strain exhibited nearly double the tungsten occupancy of enzyme isolated from its native host, indicating that synthetic control of metal uptake can rebalance endogenous W/Mo homeostatic trade-offs.

The pronounced activity loss under mixed W/Mo supplementation highlights the inherent sensitivity of W-bis-MGD maturation to W/Mo competition. Because molybdenum is not appreciably incorporated into the mature enzyme, interference likely occurs upstream of final cofactor insertion rather than through direct active-site substitution. Such cross-talk may involve competitive binding to the TupA periplasmic binding protein, limiting tungstate influx despite its higher intrinsic affinity for tungsten[40], or nonproductive engagement of the heterologous MoeA1 insertion machinery during early W-bis-MGD assembly, thereby impairing maturation of nascent cofactor intermediates[19, 20, 21]. Together, these findings position selective metal allocation and early pathway specificity as engineerable interfaces between trace-element physiology and synthetic chassis engineering.

In parallel, Fe–S cluster biogenesis represented another systems-level constraint on tungsten enzyme maturation. Because W-FDHs rely on multiple Fe–S clusters for structural integrity and electron transfer, their assembly is embedded within broader redox and metal-trafficking networks. Reinforcement of the *isc* operon relieved this bottleneck, restoring activity to native-comparable levels and enabling volumetric productivity surpassing alternative production systems[8, 34, 41], while maintaining cellular fitness. Given that Fe–S cluster assembly also contributes to early stages of bis-MGD cofactor biosynthesis[30, 31, 32], these improvements likely reflect coordinated enhancement of both electron-transfer capacity and cofactor maturation efficiency. These findings highlight that efficient production of tungsten-dependent enzymes is governed not by protein expression alone, but by integrated host metal selectivity and cofactor metabolism.

Importantly, reconstruction of tungsten-specific metal metabolism in *E. coli* preserved the intrinsic catalytic properties of MeFDH1. Although modest differences in apparent substrate affinity were observed, turnover rates between enzymes derived from the engineered *E. coli* BL2 strain and the native *M. extorquens* AM1 host remained unchanged, suggesting intact cofactor insertion and structure. Instead, they likely arise from subtle differences in local microenvironment or mediator interactions. The enhanced whole-cell CO-to-formate conversion is therefore best explained by improved maturation efficiency and increased intracellular abundance of fully active enzymes rather than altered enzyme chemistry.

The successful activation of both a canonical W-FDH (CnFDW) and a putative FDH (LbFDH) further demonstrates that the engineered chassis supports maturation across multiple W-bis-MGD–dependent enzymes rather than being tailored to a single target. Despite belonging to the same structural superfamily, these enzymes originate from evolutionarily separated bacterial lineages and were functionally restored without enzyme-specific optimization, supporting the conclusion that activation results from reconstruction of host metal metabolism rather than target-specific tuning. While validation across additional tungsten enzyme families will be important, these results establish a transferable capacity for W-bis-MGD–dependent maturation in an engineered host.

Collectively, this work extends chassis engineering beyond genetic circuit design to the rational reconfiguration of intracellular metal homeostasis. By reconciling host metal metabolism with cofactor-dependent catalysis, we establish a generalizable strategy for activating W-bis-MGD enzymes that are inaccessible in standard laboratory strains. Although demonstrated here with FDHs, the underlying design principles—coordinated control of metal uptake, cofactor biosynthesis, and auxiliary cluster assembly—provide a foundation for expanding the functional expression of tungsten-dependent redox enzymes in synthetic hosts, This platform enables aerobic production of multiple W-FDHs and establishes a general design framework for W-bis-MGD maturation, offering new opportunities to enhance biocatalytic carbon conversion and redox biomanufacturing under oxygen-tolerant conditions.

Methods

Strains, growth medium, and culture conditions

Escherichia coli DH5α was used for routine plasmid construction and propagation. *E. coli* BL21(DE3) served as the parental strain for heterologous protein expression and all subsequent chassis engineering. All strains and plasmids used in this study are listed in Table 1. Seed cultures were initiated in Luria–Bertani (LB) medium (10 g L^{-1} tryptone, 5 g L^{-1} yeast extract, 10 g L^{-1} NaCl) supplemented, where appropriate, with carbenicillin (100 μg mL^{-1}) or spectinomycin (100 μg mL^{-1}). For protein expression, cultures were transferred to Terrific Broth (TB; 12 g L^{-1} tryptone, 24 g L^{-1} yeast extract, 9.4 g L^{-1} K_2HPO_4, 2.2 g L^{-1} KH_2PO_4) with appropriate antibiotics. Sodium tungstate (Na_2WO_4) was added to a final concentration of 1 mM, and $FeSO_4$ (1 mM) was included where indicated.

Plasmid construction

All heterologous genes were codon-optimized for *E. coli* expression and synthesized commercially by Bionics (Seoul, Republic of Korea). The identity and putative function of each heterologous gene used in this study are summarized in Supplementary **Table S3**. Gene fragments were assembled into the indicated plasmid backbones using Gibson Assembly Master Mix (New England Biolabs, MA, USA) following the manufacturer's instructions. All constructs were propagated in *E. coli* DH5α and verified by colony PCR and Sanger sequencing prior to use.

MeFDH1 expression vectors were constructed by assembling *Methylorubrum extorquens* AM1 genes *fdh1A* and *fdh1B* into the pETDuet-1 backbone under separate T7 promoters. Expression vectors for *Cupriavidus necator* H16 *fdwAB* and *Lutibaculum baratangense* AMV1 *fdhAB* were constructed similarly in the pETDuet-1 backbone. Genes involved in W-bis-MGD biosynthesis (*moeA1*, *mobB*, *mobA*, and *fdhD*) were assembled individually or in defined combinations into pCDFDuet-1 under T7 promoters to enable modular co-expression.

For comparative analysis of tungstate uptake systems, the *modABC* operon from *E. coli* K-12 was amplified from genomic DNA using Q5® High-Fidelity DNA Polymerase (New England Biolabs, MA, USA), while the *tupBCA* operons from *M. extorquens* AM1 and *Sulfitobacter dubius* NA4 were codon-optimized and synthesized. All transporter operons were cloned into the pZS vector for plasmid-based expression.

Strain engineering

All strain engineering was performed in *E. coli* BL21(DE3). For transporter engineering, the *tupBCA* operon from *S. dubius* NA4 was chromosomally integrated using λ-Red recombination. The operon was inserted into the *proP* locus using the pKD4/pRedET system, followed by excision of the selection marker with the pCP20 plasmid. The resulting strain carrying chromosomally encoded *tupBCA* was designated BL1.

To enhance Fe–S cluster biosynthesis, *iscR* was deleted and the native *isc* promoter was replaced with the synthetic P*trc* promoter via the two-step inactivation method using the pKOV plasmid [42]. The final engineered strain incorporating chromosomal *tupBCA* and upregulated *isc* expression was designated BL2 and used as the expression chassis in subsequent protein expression and activity assays. All genomic modifications were validated by colony PCR and verified by Sanger sequencing.

Protein expression and purification

Recombinant *E. coli* strains were cultivated by inoculating 1:100 dilutions of overnight seed cultures into 200 mL of TB medium in 1 L baffled flasks. Cultures were incubated at 37°C with shaking to mid-exponential phase (OD_{600} ≈ 0.5–0.6), and protein expression was induced with 0.1 mM isopropyl β-D-1-thiogalactopyranoside (IPTG). Following induction, cells were incubated at 25°C for 16–20 h. All cultivation and protein expression experiments were performed under aerobic conditions.

Cell lysis and protein purification were also conducted aerobically. Cells were harvested by centrifugation at 7,000 × g for 15 min at 4°C and resuspended in BugBuster Protein Extraction Reagent (Millipore Sigma) and lysed according to the manufacturer's protocol. Lysates were clarified by a second centrifugation step at 11,000 × g for 30 min at 4°C.

Recombinant enzymes were purified from the soluble fraction using nickel-nitrilotriacetic acid (Ni-NTA) affinity chromatography. Column was equilibrated and washed with 50 mM MOPS buffer (pH 7.0) containing 250 mM NaCl and 20 mM imidazole, and bound proteins were eluted with 300 mM imidazole in the same buffer. Protein concentrations were determined spectrophotometrically (NanoDrop, Thermo

Scientific) using calculated extinction coefficient specific to each enzyme (ε = 8.94 L·mg⁻¹·cm⁻¹ for MeFDH1, ε = 8.07 L·mg⁻¹·cm⁻¹ for CnFDW, and ε = 9.59 L·mg⁻¹·cm⁻¹ for LbFDH).

Enzyme activity assays

Enzyme activity was measured spectrophotometrically by monitoring NAD^+ reduction at 340 nm (ε = 6.22 $mM^{-1}·cm^{-1}$) using a UV–Vis spectrophotometer under aerobic conditions. Assays were conducted in quartz cuvettes with a total volume of 2.0 mL at 30°C. The standard reaction mixture contained 50 mM MOPS buffer (pH 7.0), 30 mM potassium formate, 0.5 mM NAD^+, and 10–20 µg of purified enzyme. One unit (U) of activity was defined as the amount of enzyme catalyzing the formation of 1 µmol NADH per minute under these conditions.

Metal content analysis

The tungsten, molybdenum, and iron contents of purified enzymes were quantified using inductively coupled plasma–mass spectrometry (ICP-MS). Approximately 1 mL of each protein sample (1.0–2.0 mg mL^{-1}) was subjected to acid digestion in Teflon vessels containing 12 mL of trace metal–grade nitric acid (HNO_3) and 1 mL of hydrofluoric acid (HF). Digestion was carried out at 200°C for 2–3 h. After cooling to room temperature, the digested samples were diluted to a final volume of 25 mL with 1% HNO_3. Metal concentrations were measured using a PerkinElmer NexION 5000 ICP-MS calibrated against PerkinElmer multi-element standards 3 and 5. Measured values were normalized to protein concentration and expressed as molar equivalents of metal per αβ heterodimer.

Kinetic analysis of MeFDH1 for CO_2 reduction

CO_2-reduction kinetics were measured anaerobically using reduced ethyl viologen ($EV^{•+}$) as the electron donor, monitored spectrophotometrically at 600 nm (ε = 10.22 mM^{-1} cm^{-1}). All assays were conducted inside an anaerobic chamber to prevent the abiotic oxidation of $EV^{•+}$ by oxygen, which would otherwise result in overestimated reaction rates. Reaction mixtures contained phosphate buffer (200 mM, pH 6.3), $EV^{•+}$ (0.015–0.12 mM), and bicarbonate (3–100 mM).

Sodium bicarbonate served as the CO_2 source and the relative concentrations of dissolved CO_2(aq), bicarbonate (HCO_3^-), and carbonate (CO_3^{2-}) were calculated from the total inorganic carbon concentration (c) according carbonate equilibrium relationships[43], using dissociation constants pKa_1 = 6.3 and pKa_2 = 10.3:

$$[CO_2(aq)] = \frac{c[H^+]^2}{[H^+]^2+[H^+]K_{a1}+K_{a1}K_{a2}} \quad (1)$$

$$[HCO_3^-] = \frac{c[H^+]K_{a1}}{[H^+]^2+[H^+]K_{a1}+K_{a1}K_{a2}} \quad (2)$$

$$[CO_3^{2-}] = \frac{cK_{a1}K_{a2}}{[H^+]^2+[H^+]K_{a1}+K_{a1}K_{a2}} \quad (3)$$

Initial rates (v_0) were determined from the linear portion of absorbance traces. Kinetic parameters (kcat, K_M, and kcat/K_M) were obtained by nonlinear regression of v_0 versus substrate concentration to the Michaelis–Menten equation using OriginPro. Representative kinetic curves and model fits are shown in Supplementary **Fig. S7**.

Whole-cell CO-to-formate conversion

Whole-cell formate production was evaluated using MeFDH1 expressed in either *E. coli* or *M. extorquens* AM1. The biocatalytic system consisted of two components: (i) an *E. coli* strain expressing carbon monoxide dehydrogenase from *Carboxydothermus hydrogenoformans* (ChCODH) and (ii) either *E. coli* expressing MeFDH1 or *M. extorquens* AM1 cells expressing MeFDH1. The two cell populations were combined at a fixed CODH-to-FDH activity ratio of 1:10 based on cell dry weight equivalents.

Reactions were performed under anaerobic conditions in 10-mL serum vials continuously sparged with CO/CO_2 gas mixture (1:1, v/v) at 3 vvm. The reaction mixture was maintained at pH 6.5, and ethyl viologen (EV) was added to a final concentration of 10 mM as an electron mediator. Whole-cell biotransformations were conducted for 4 h at 30°C with continuous agitation to ensure homogeneous gas–liquid transfer.

Formate concentrations were quantified by high-performance liquid chromatography (HPLC) using an Aminex HPX-87H column (Bio-Rad) operated at 35°C, with 5 mM H_2SO_4 at a flow rate of 0.6 mL min^{-1} and detection using a refractive index (RI) detector. Calibration curves were generated using authentic sodium formate standards over a concentration range of 0–500 mM.

Statistical analysis and reproducibility

Statistical analyses were performed using OriginPro. All experiments were conducted with at least three independent replicates unless otherwise stated. Data are presented as mean ± standard deviation (s.d.), as indicated in the figure legends. Statistical significance was evaluated using an unpaired two-tailed Student's *t*-test, and *P* values < 0.05 were considered statistically significant. Nonlinear regression for kinetic parameters (kcat and K_M) was performed by unweighted least-squares fitting to the Michaelis–Menten equation. No statistical methods were used to predetermine sample size. No data were excluded from the analysis. Experiments were not randomized, and investigators were not blinded to group allocation during experiments or outcome assessments.

Declarations

Data availability

Data supporting the findings of this study are available within the Article and its Supplementary Information files and source data are provided with this paper.

Acknowledgements

This research was supported by the National Research Foundation of Korea (NRF), funded by the Ministry of Science, ICT & Future Planning (RS-2020-NR049543, RS-2024-00396026, RS-2024-00466474, RS-2024-00453085, RS-2025-16070008). We thank UNIST Central Research Facilities for assistance with ICP-MS measurements and access to instrumentation.

Author contribution

U. T. P.: Conceptualization, validation, formal analysis, investigation, writing – original draft, writing – review, and editing. **J.-M. L.**: Conceptualization, validation, formal analysis, investigation, writing – original draft, writing – review, and editing. **T. M. V.**: formal analysis, investigation. **M.-K. O.**: Supervision, project administration, formal analysis, writing – original draft, writing – review, and editing. **Y. H. K.**: Supervision, project administration, formal analysis, writing – original draft, writing – review, and editing.

Competing interests

The authors declare no competing interests.

References

1. Birdja YY et al (2019) Advances and challenges in understanding the electrocatalytic conversion of carbon dioxide to fuels. Nat Energy 4:732–745
2. Lai W, Qiao Y, Zhang J, Lin Z, Huang H (2022) Design strategies for markedly enhancing energy efficiency in the electrocatalytic CO2 reduction reaction. Energy Environ Sci 15:3603–3629
3. Sordakis K et al (2018) Homogeneous catalysis for sustainable hydrogen storage in formic acid and alcohols. Chem Rev 118:372–433
4. Bar-Even A (2016) Formate assimilation: the metabolic architecture of natural and synthetic pathways. Biochemistry 55:3851–3863
5. Zhang L, Liu J, Ong J, Li SF (2016) Specific and sustainable bioelectro-reduction of carbon dioxide to formate on a novel enzymatic cathode. Chemosphere 162:228–234
6. Alissandratos A, Kim HK, Easton CJ (2014) Formate production through carbon dioxide hydrogenation with recombinant whole cell biocatalysts. Bioresour Technol 164:7–11
7. Niks D, Hille R (2019) Molybdenum- and tungsten-containing formate dehydrogenases and formylmethanofuran dehydrogenases: structure, mechanism, and cofactor insertion. Protein Sci 28:111–122
8. Laukel M, Chistoserdova L, Lidstrom ME, Vorholt JA (2003) The tungsten-containing formate dehydrogenase from *Methylobacterium extorquens* AM1: purification and properties. Eur J Biochem 270:325–333
9. Seelmann CS, Willistein M, Heider J, Boll M (2020) Tungstoenzymes: occurrence, catalytic diversity and cofactor synthesis. Inorganics 8:44

10. Majumdar A (2014) Structural and functional models in molybdenum and tungsten bioinorganic chemistry: description of selected model complexes, present scenario and possible future scopes. Dalton Trans 43:8990–9003
11. Hille R, Hall J, Basu P (2014) The mononuclear molybdenum enzymes. Chem Rev 114:3963–4038
12. Bevers LE, Hagedoorn P-L, Hagen WR (2009) The bioinorganic chemistry of tungsten. Coord Chem Rev 253:269–290
13. Raaijmakers H et al (2002) Gene sequence and the 1.8 Å crystal structure of the tungsten-containing formate dehydrogenase from *Desulfovibrio gigas*. Structure 10:1261–1272
14. Schulz M et al (2025) Functional expression of a Mo-dependent formate dehydrogenase in *Escherichia coli* under aerobic conditions. PLoS ONE 20:e0334613
15. Cowan AE et al (2025) Fast growth and high-titer bioproduction from renewable formate via metal-dependent formate dehydrogenase in *Escherichia coli*. Nat Commun 16:5908
16. Shi HL et al (2024) Engineered *Escherichia coli* whole cell-mediated electro-biocatalysis for carbon dioxide to formic acid conversion. ACS Sustain Chem Eng 12:5544–5554
17. Liu W et al (2024) Bioelectrocatalytic carbon dioxide reduction by an engineered formate dehydrogenase from *Thermoanaerobacter kivui*. Nat Commun 15:9962
18. Szaleniec M, Heider J (2025) Obligately tungsten-dependent enzymes—catalytic mechanisms, models and applications. Biochemistry 64:2154–2172
19. Ryu H, Nguyen CNM, Lee SK, Park S (2024) Development of *Cupriavidus necator* H16 as a host for heterologous production of formate dehydrogenase I of *Methylorubrum extorquens*: possibilities and limitations. Bioresour Technol 394:130187
20. Bevers LE et al (2008) Function of MoaB proteins in the biosynthesis of the molybdenum and tungsten cofactors. Biochemistry 47:949–956
21. Leimkühler S (2023) Metal-containing formate dehydrogenases, a personal view. Molecules 28:5338
22. Park J et al (2024) Structure of recombinant formate dehydrogenase from *Methylobacterium extorquens* (MeFDH1). Sci Rep 14:3819
23. Pinske C, Bonn M, Kruger S, Lindenstrauss U, Sawers RG (2011) Metabolic deficiencies revealed in the biotechnologically important model bacterium *Escherichia coli* BL21(DE3). PLoS ONE 6:e22830
24. Han MJ (2016) Exploring the proteomic characteristics of the *Escherichia coli* B and K-12 strains in different cellular compartments. J Biosci Bioeng 122:1–9
25. Coimbra C, Branco R, Morais PV (2019) Efficient bioaccumulation of tungsten by *Escherichia coli* cells expressing the *Sulfitobacter dubius* TupBCA system. Syst Appl Microbiol 42:126001
26. Coimbra C, Farias P, Branco R, Morais PV (2017) Tungsten accumulation by highly tolerant marine hydrothermal *Sulfitobacter dubius* strains carrying a *tupBCA* cluster. Syst Appl Microbiol 40:388–395
27. Vuilleumier S et al (2009) Methylobacterium genome sequences: a reference blueprint to investigate microbial metabolism of C1 compounds from natural and industrial sources. PLoS ONE 4:e5584

28. Outten FW, Djaman O, Storz G (2004) A *suf* operon requirement for Fe–S cluster assembly during iron starvation in *Escherichia coli*. Mol Microbiol 52:861–872
29. Mettert EL, Kiley PJ (2014) Coordinate regulation of the Suf and Isc Fe–S cluster biogenesis pathways by IscR is essential for viability of *Escherichia coli*. J Bacteriol 196:4315–4323
30. Zupok A, Iobbi-Nivol C, Mejean V, Leimkühler S (2019) The regulation of Moco biosynthesis and molybdoenzyme gene expression by molybdenum and iron in bacteria. Metallomics 11:1602–1624
31. Mendel RR, Hercher TW, Zupok A, Hasnat MA, Leimkühler S (2020) The requirement of inorganic Fe–S clusters for the biosynthesis of the organometallic molybdenum cofactor. Inorganics 8:43
32. Leimkühler S (2021) Transition metals in catalysis: the functional relationship of Fe–S clusters and molybdenum or tungsten cofactor-containing enzyme systems. Inorganics 9:6
33. Nakamura M, Saeki K, Takahashi Y (1999) Hyperproduction of recombinant ferredoxins in *Escherichia coli* by coexpression of the ORF1-ORF2-iscS-iscU-iscA-hscB-hscA-fdx-ORF3 gene cluster. J Biochem 126:10–18
34. Ryu H et al (2025) Production and characterization of CO2 reducing and tungsten-containing formate dehydrogenase of *Cupriavidus necator* H16. Biotechnol Bioprocess Eng 30:363–376
35. van Kempen M et al (2024) Fast and accurate protein structure search with Foldseek. Nat Biotechnol 42:243–246
36. Leimkühler S (2020) The biosynthesis of the molybdenum cofactors in *Escherichia coli*. Environ Microbiol 22:2007–2026
37. Magalon A, Mendel RR (2008) Biosynthesis and insertion of the molybdenum cofactor. EcoSal Plus 3
38. Bevers LE, Schwarz G, Hagen WR (2011) A molecular basis for tungstate selectivity in prokaryotic ABC transport systems. J Bacteriol 193:4999–5001
39. Hagen WR (2011) Cellular uptake of molybdenum and tungsten. Coord Chem Rev 255:1117–1128
40. Otrelo-Cardoso AR et al (2017) Highly selective tungstate transporter protein TupA from *Desulfovibrio alaskensis* G20. Sci Rep 7:5798
41. Jang J, Jeon BW, Kim YH (2018) Bioelectrochemical conversion of CO2 to value added product formate using engineered *Methylobacterium extorquens*. Sci Rep 8:7211
42. Link AJ, Phillips D, Church GM (1997) Methods for generating precise deletions and insertions in the genome of wild-type *Escherichia coli*: application to open reading frame characterization. J Bacteriol 179:6228–6237
43. Jeon BW et al (2024) Enzymatic conversion of CO2 to formate: the potential of tungsten-containing formate dehydrogenase in flow reactor system. J CO2 Util 82:102754

Tables

Table 1. Strains and plasmids used in this study.

Strains	Description	Source/Reference
BL21(DE3)	*E. coli* BL21(DE3) expression host	RBC Real Biotech
BL	BL21(DE3) expressing *Methylorubrum extorquens* FDH1	This study
BL(W1)	BL21(DE3) expressing MeFDH1 with MoeA1	This study
BL(WA)	BL21(DE3) expressing MeFDH1 with MobA	This study
BL(WB)	BL21(DE3) expressing MeFDH1 with MobB	This study
BL(W2)	BL21(DE3) expressing MeFDH1 with MoeA1 and MobB	This study
BL(W3)	BL21(DE3) expressing MeFDH1 with MoeA1, MobA and MobB	This study
BL(W4)	BL21(DE3) expressing MeFDH1 with MoeA1, MobA, MobB and FdhD (W4 machinery)	This study
BL1	BL21(DE3) with chromosomal tungstate transporter (*ΔproP*::PT7–*tupBCA* from *Sulfitobacter dubius* NA4)	This study
BL1(W4)	BL1 expressing MeFDH1 with W4 machinery	This study
BL1(W4+ISC)	BL1(W4) harboring pRKISC (*isc* operon)	This study
BL2	BL1 with chromosomally upregulated isc operon (*ΔiscR*::*Ptrc*–*iscSUA*–*hscBA*–*fdx*)	This study
BL2(W4)	BL2 expressing MeFDH1 with W4 machinery	This study
BL(Cn)	BL expressing *Cupriavidus necator* FDW	This study
BL2(W4+Cn)	BL2 expressing CnFDW together with W4 machinery	This study
BL(Lb)	BL expressing *Lutibaculum baratangense* FDH	This study
BL2(W4+Lb)	BL2 expressing LbFDH together with W4 machinery	This study
Plasmids	**Description**	**Source/Reference**

pETDuet-1	Dual T7 expression backbone, Amp	Expressys
pF1	pETDuet-1 carrying *M. extorquens* FDH1 α/β expression cassette (*fdh1A*-6×His–*fdh1B*)	This study
pF2	pETDuet-1 carrying *C. necator* FDW α/β expression cassette (*fdwA*-6×His–*fdwB*)	This study
pF3	pETDuet-1 carrying *L. baratangense* FDH α/β expression cassette (*fdhA*-6×His–*fdhB*)	This study
pCDFDuet-1	Cloning/expression backbone, Sm	Expressys
pW1	pCDFDuet-1 carrying *moeA1* from *M. extorquens* AM1	This study
pWA	pCDFDuet-1 carrying *mobA* from *M. extorquens* AM1	This study
pWB	pCDFDuet-1 carrying *mobB* from *M. extorquens* AM1	This study
pW1A	pCDFDuet-1 carrying *moeA1–mobA* from *M. extorquens* AM1	This study
pW1B	pCDFDuet-1 carrying *moeA1–mobB* from *M. extorquens* AM1	This study
pWAB	pCDFDuet-1 carrying *mobA–mobB* from *M. extorquens* AM1	This study
pW3	pCDFDuet-1 carrying *moeA1–mobA–mobB* from *M. extorquens* AM1	This study
pW4	pCDFDuet-1 carrying *moeA1–mobA–mobB–fdhD* from *M. extorquens* AM1	This study
pZ1	pZS21 carrying *modABC* from *E. coli* K-12	This study
pZ2	pZS21 carrying *tupBCA* from *S. dubius* NA4	This study
pZ3	pZS21 carrying *tupBCA* from *M. extorquens* AM1	This study
pRKISC	*iscSUA–hscBA–fdx* operon, Tet	Nakamura *et al*.[33]

Table 2. Metal content of MeFDH1 across engineered *E. coli* strains and the native *M. extorquens* AM1 host.

Metal incorporation into purified MeFDH1 was quantified by inductively coupled plasma–mass spectrometry (ICP–MS). Iron (Fe), tungsten (W), and molybdenum (Mo) contents are shown for enzymes produced in strains expressing progressively expanded tungsten-cofactor biosynthetic and accessory modules: BL (MeFDH1 only), BL(W4) (MoeA1, MobA, MobB and FdhD), BL1(W4) (W4 machinery with chromosomal *tupBCA*), BL1(W4+ISC) (additional plasmid-borne *isc* operon), BL2(W4) (chromosomally upregulated *isc* operon), and the native AM1 host. Values represent mean ± s.d. (n = 3).

Strain	Metal content (mol metal mol^{-1} enzyme)		
	Fe	W	Mo
BL	1.75 ± 0.03	0.01 ± 0.01	0.02 ± 0.01
BL(W4)	5.50 ± 0.09	0.27 ± 0.05	0.05 ± 0.04
BL1(W4)	5.14 ± 0.10	0.55 ± 0.05	0.09 ± 0.05
BL1(W4+ISC)	8.30 ± 0.10	0.75 ± 0.03	0.05 ± 0.05
BL2(W4)	10.8 ± 0.09	0.92 ± 0.01	0.02 ± 0.01
AM1	11.6 ± 0.21	0.50 ± 0.05	0.02 ± 0.02

Table 3. Kinetic parameters of MeFDH1 in expressed engineered *E. coli* compared with the enzyme from *M. extorquens* AM1

Turnover numbers (k_{cat}), Michaelis constants (K_M), and catalytic efficiencies (k_{cat}/K_M) were determined for CO_2 reduction using either dissolved CO_2 or reduced ethyl viologen ($EV^{+\cdot}$) as the electron mediator. MeFDH1 was purified from *E. coli* BL2 (BL2) or isolated from the native AM1 host. Values represent mean ± s.d. (n = 3).

		k_{cat} (s^{-1})	K_M (mM)	k_{cat}/K_M (s^{-1} mM^{-1})
CO_2	BL2	141 ± 10	8.4 ± 1.4	17 ± 3
	AM1	152 ± 5	3.6 ± 0.1	42 ± 1
$EV^{\bullet+}$	BL2	304 ± 39	0.06 ± 0.02	5067 ± 1810
	AM1	325 ± 6	0.02 ± 0.01	16250 ± 8131

Table 4. Functional expression of heterologous tungsten-dependent dehydrogenases in engineered *E. coli* chassis.

CnFDW from *C. necator* H16 and LbFDH from *L. baratangense* AMV1 were expressed in BL21(DE3) or the engineered BL2 chassis. BL2 carries a chromosomally integrated tungstate transporter (*tupBCA*), chromosomal upregulation of the isc operon, and plasmid-encoded W-cofactor biosynthetic genes (*moeA1*, *mobA*, *mobB*, and *fdhD*). Specific activities were determined by enzymatic assay, and metal contents (Fe, W, Mo) were quantified by ICP–MS. ND, not detected. Values represent mean ± s.d. (n = 3).

Strain	Specific activity	Metal (mol mol⁻¹ enzyme)		
	(U mg⁻¹ enzyme)	Fe	W	Mo
BL(Cn)	ND	2.72 ± 0.01	0.03 ± 0.01	0.04 ± 0.01
BL2(W4+Cn)	38 ± 4	18.6 ± 0.02	0.89 ± 0.02	0.03 ± 0.02
BL(Lb)	ND	5.68 ± 0.08	0.01 ± 0.01	0.24 ± 0.01
BL2(W4+Lb)	8 ± 3	12.8 ± 0.04	1.17 ± 0.02*	0.01 ± 0.01

* W occupancy slightly above 1.0 reflects minor analytical uncertainty in protein quantification.

Figures

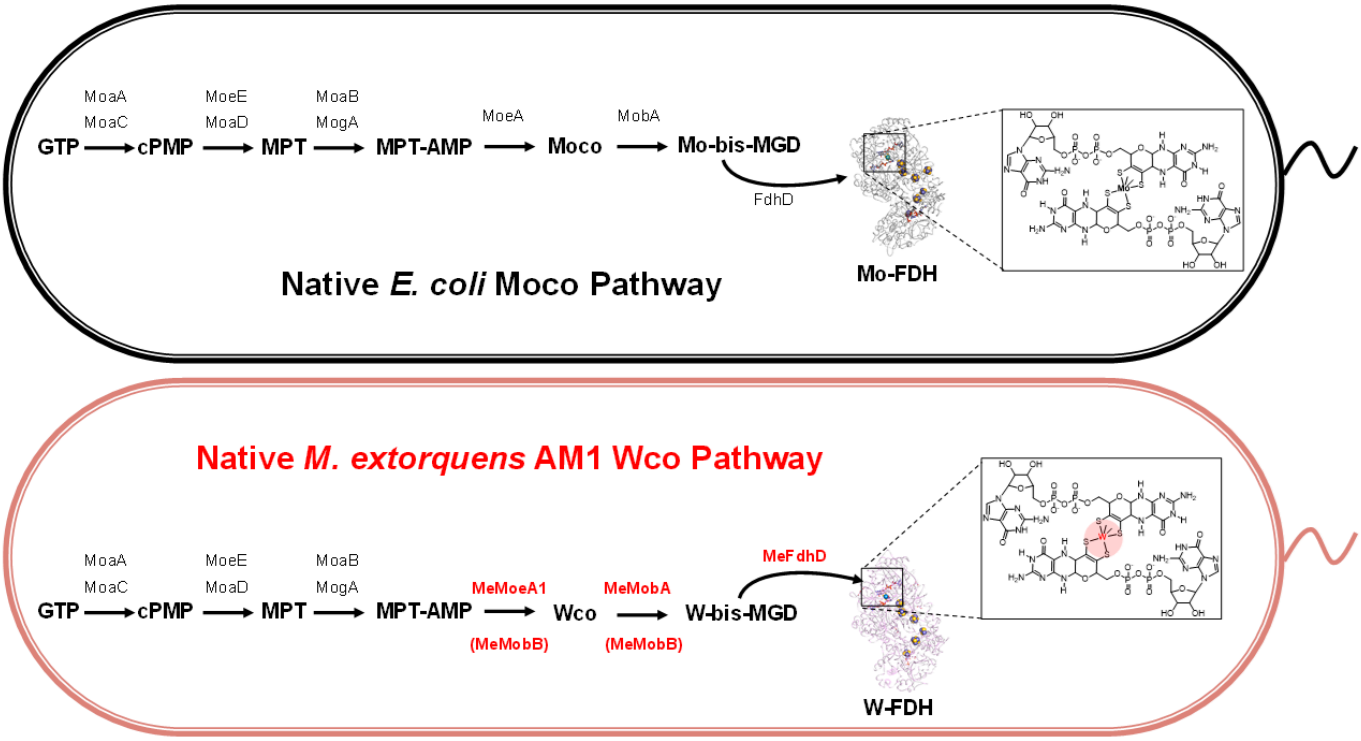


Figure 1

Comparative biogenesis of molybdenum- and tungsten-containing bis-MGD cofactors.

Schematic comparison of Mo-bis-MGD biosynthesis in native Escherichia coli and W-bis-MGD biosynthesis in M. extorquens AM1. *The native E. coli pathways support molybdenum insertion but is incompatible with tungsten-dependent enzymes.* In contrast, the *M. extorquens* AM1 pathway, involving MoeA1, MobA, MobB and FdhD, enables selective tungstate incorporation, guanylylation and sulfur transfer, resulting in the formation of catalytically competent W-bis-MGD.

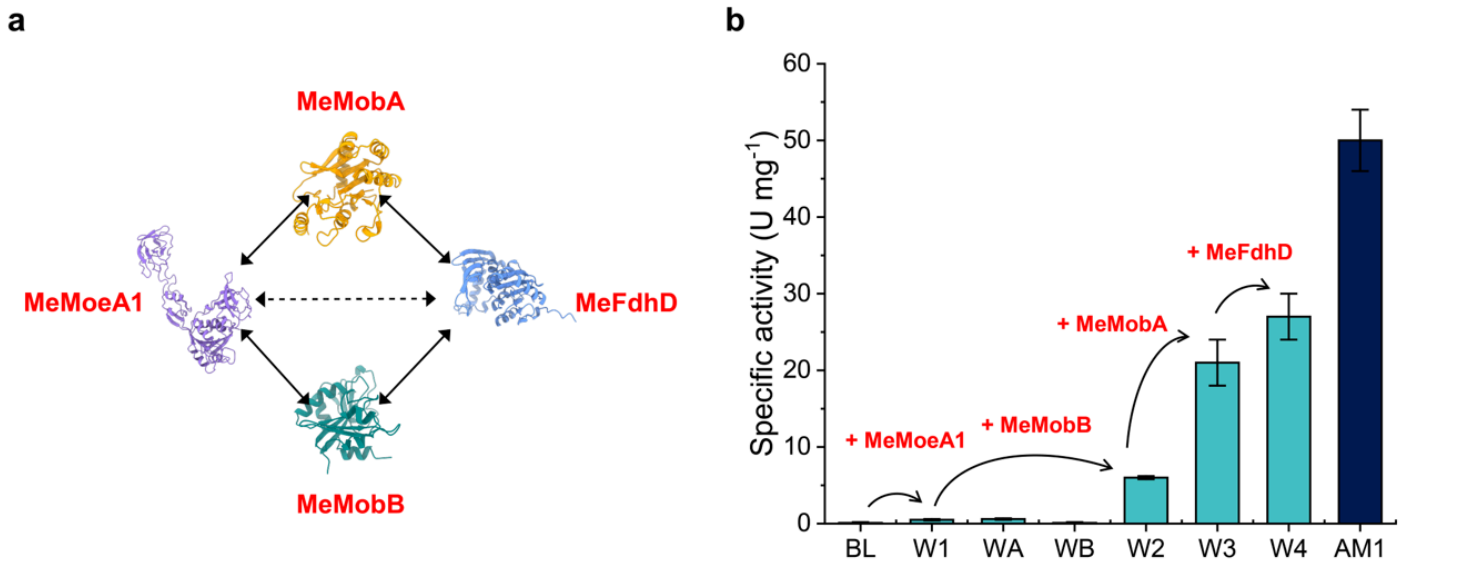


Figure 2

Stepwise reconstitution of the tungsten-cofactor (Wco) biosynthetic pathway and its impact on MeFDH1 activity in *E. coli*BL21(DE3).

a, Schematic representation of the reconstructed W-bis-MGD maturation pathway.AlphaFold3-predicted structures of MoeA1, MobA, MobB, and FdhD from *M. extorquens*AM1 were arranged to reflect interaction relationships observed in the BACTH assay (Supplementary Fig. S1). Strong interactions between MoeA1–MobA and MoeA1–MobB (solid lines) indicate a tightly associated core complex for W-bis-MGD biogenesis, whereas the weaker MoeA1–FdhD interaction (dashed line) suggests transient recruitment, consistent with sulfur transfer to the nascent cofactor.
b, Specific activity of recombinant MeFDH1 expressed in *E. coli* BL21(DE3) with stepwise combinations of Wco biosynthetic genes: BL (MeFDH1 only), W1 (+MoeA1), WA (+MobA), WB (+MobB), W2 (+MoeA1+MobB), W3 (+MoeA1+MobA+MobB), and W4 (+MoeA1+MobA+MobB+FdhD). Activity of MeFDH1 in the native *M. extorquens* AM1 host is shown for comparison. Bars represent mean ± s.d. (n = 3).

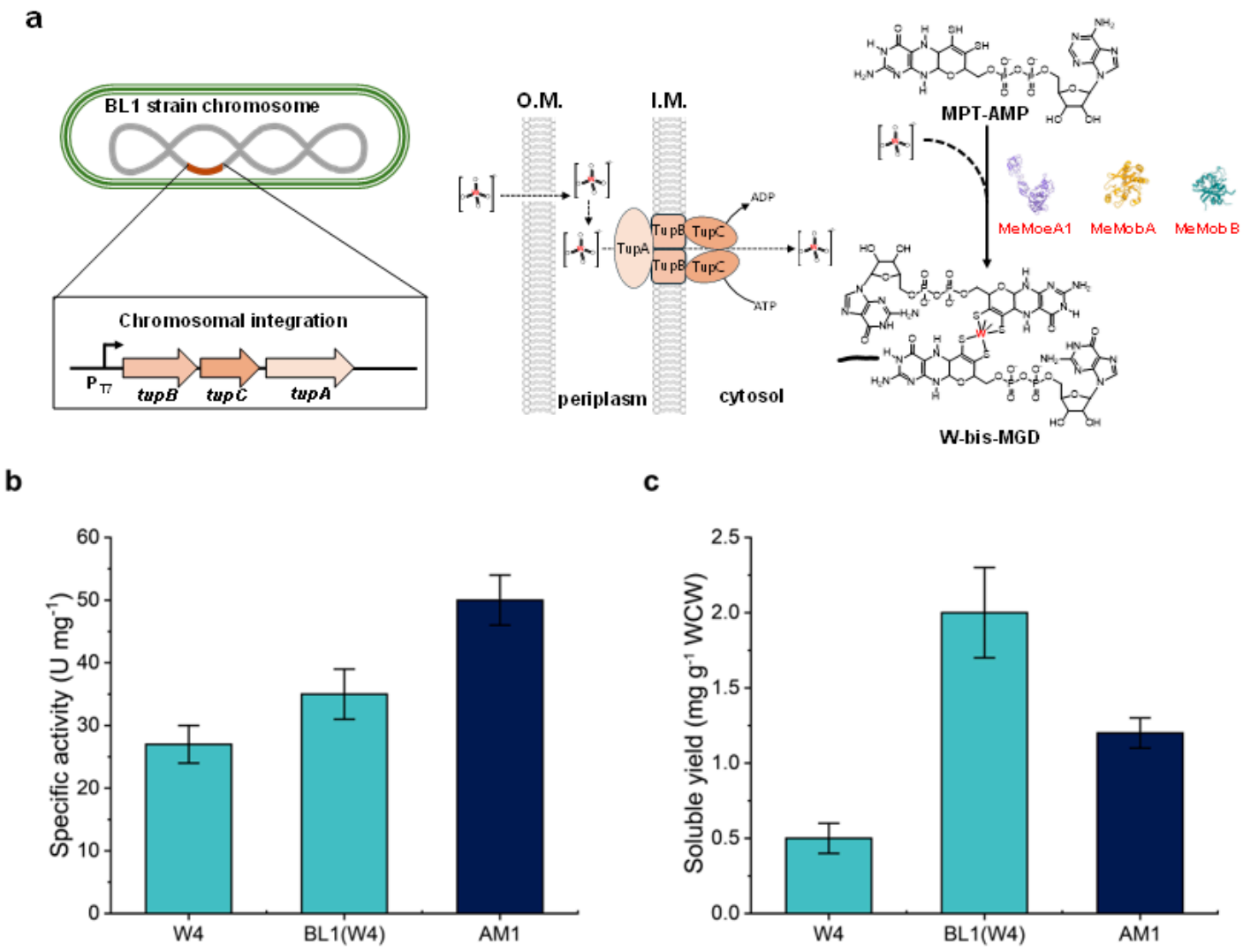


Figure 3

Chromosomal expression of the TupBCA transporter enhances tungstate uptake and MeFDH1 maturation in *E. coli*.

a, Schematic of heterologous chromosomal integration of the *Sulfitobacter dubius* NA4 *tupBCA* operon, encoding a high-affinity tungstate transport system. This modification facilitates tungsten uptake across the cell membrane, supporting intracellular cofactor biosynthesis and activation of W-dependent enzymes such as MeFDH1.

b, Specific activity (U mg^{-1}) of MeFDH1 expressed in *E. coli* BL21(DE3) carrying the W4 biosynthetic module alone (W4) or combined with chromosomal *tupBCA* [BL1(W4)], compared with the native *M. extorquens* AM1 host.

c, Corresponding soluble MeFDH1 yield (mg g^{-1} WCW). Data represent mean ± s.d. (n = 3).

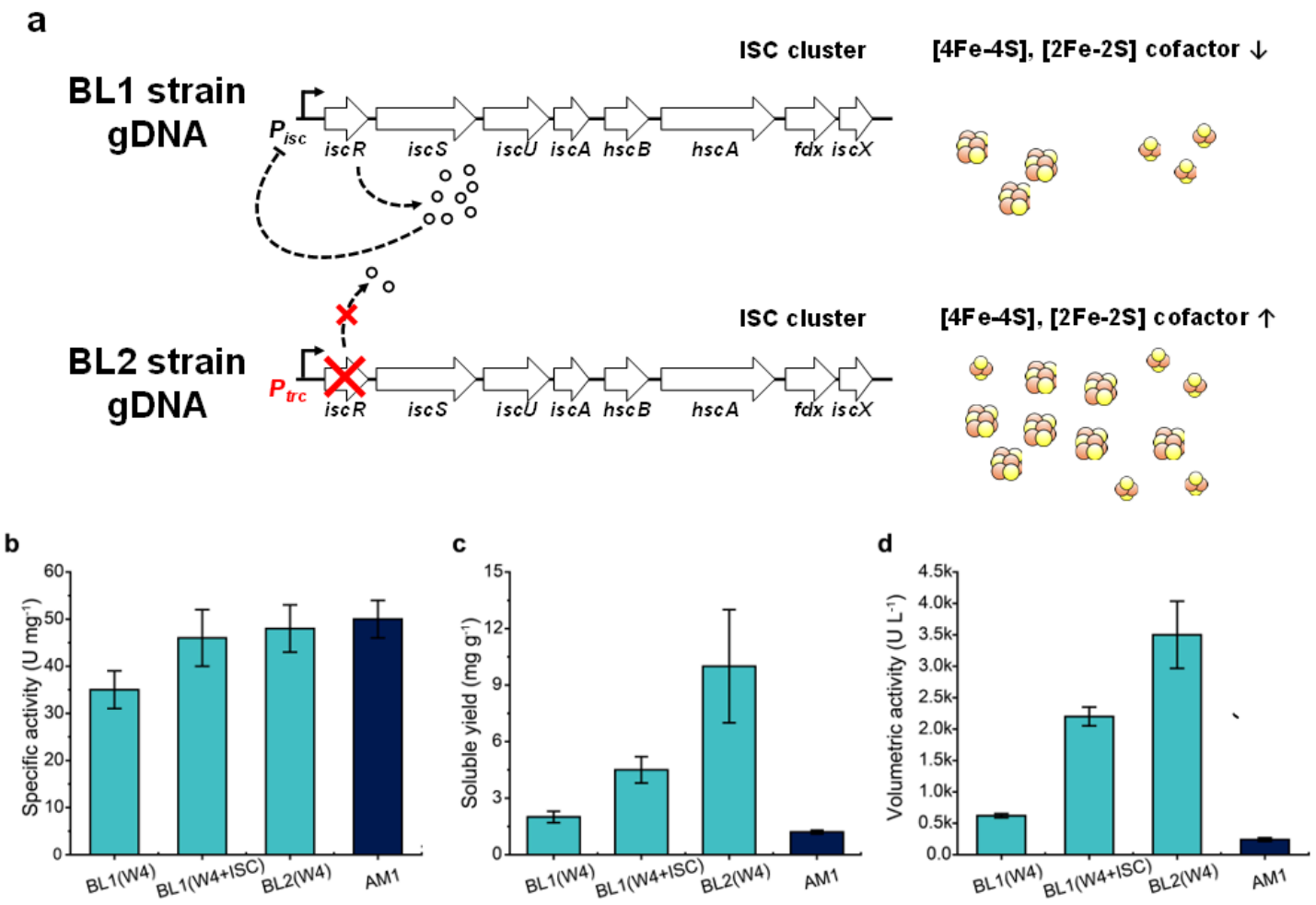


Figure 4

Reinforcement of Fe–S cluster biogenesis further enhances MeFDH1 performance in engineered *E. coli*.

a,Schematic of enhancement of the *isc* pathway through deletion of the transcriptional repressor *iscR* and *Ptrc*-driven expression of the *iscSUA–hscBA–fdx*operon, increasing cellular Fe–S cluster assembly capacity.

b–d, Specific activity, soluble protein yield, and volumetric activity of MeFDH1 expressed in *E. coli* strains with stepwise optimization of Fe–S cluster biogenesis: BL1(W4) (chromosomal *tupBCA*), BL1(W4+ISC) (plasmid-borne *isc* operon), and BL2(W4) (chromosomally upregulated *isc* operon), compared with the native *M. extorquens* AM1 host. Bars represent mean ± s.d. (n = 3).

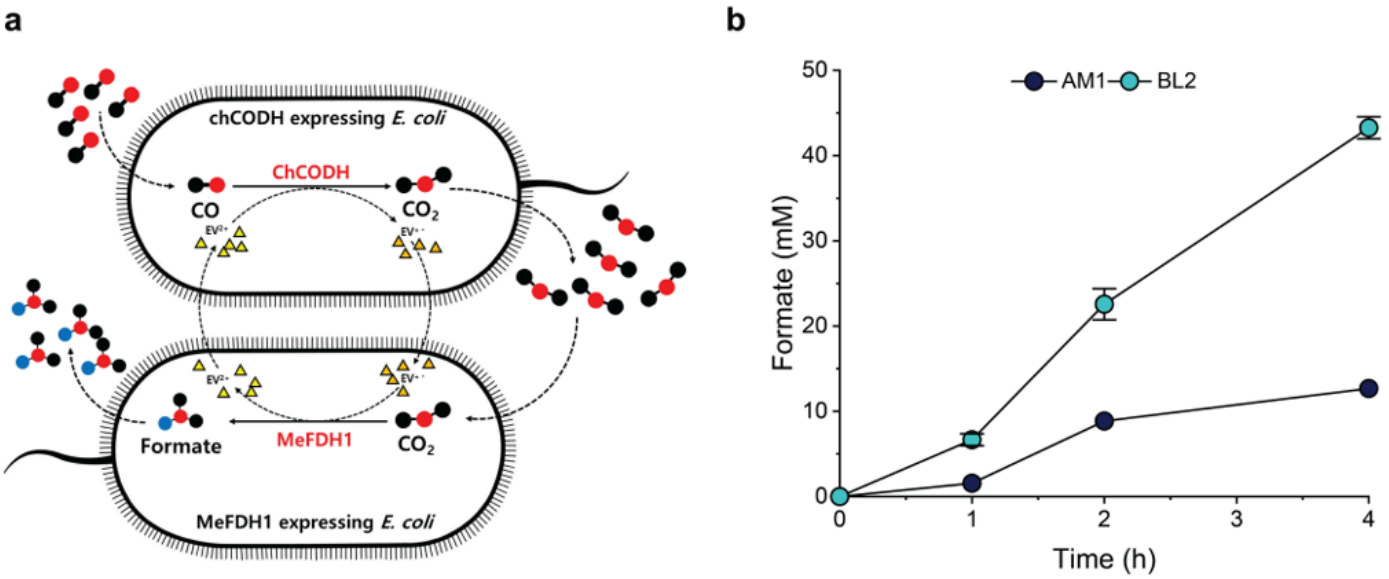


Figure 5

Whole-cell CO-to-formate conversion using MeFDH1 expressed in engineered *E. coli* BL2 and the native *M. extorquens* AM1 host.
a, Schematic of the coupled whole-cell system. *E. coli* expressing ChCODH oxidizes CO to CO_2, generating reduced ethyl viologen ($EV^{\bullet+}$), which mediates electron transfer to *E. coli* expressing MeFDH1 and drives the reductive conversion of CO_2 to formate. Oxidized EV^{2+} is recycled back to the ChCODH-expressing cells, completing the electron-transfer cycle.
b, Time course of formate production in the coupled system using ChCODH-expressing cells combined with MeFDH1 produced in either *E. coli* BL2 or *M. extorquens* AM1. Cell densities were normalized based on dry weight equivalents. Data represent mean ± s.d.(n = 3).

Supplementary Files

This is a list of supplementary files associated with this preprint. Click to download.

- 260219SImeFDH1E.colifinalversion.docx